Scanning Microscopy Vol. 13, No. 1, 1999 (Pages 147-157) 0891-703599$5.00+.25
Scanning Microscopy International, Chicago (AMF O'Hare), IL 60666 USA

QUANTITATIVE IMAGING AND ANALYSIS OF BIOLOGICAL SPECIMENS IN THE FIELD-EMISSION SCANNING TRANSMISSION ELECTRON MICROSCOPE: CAPABILITIES AND LIMITATIONS

S. Brian Andrews[1]*, Natalia B. Pivovarova[1] and Richard D. Leapman[2]

[1]Laboratory of Neurobiology, NINDS, and [2]Bioengineering and Physical Science Program, ORS, National Institutes of Health, Bethesda, MD 20892

(Received for publication June 18, 1998 and in revised form November 23, 1998)

Abstract

We have been applying a field-emission scanning transmission electron microscope (STEM) to high-resolution imaging and analysis of biological specimens. This instrument is equipped with a cold/cryotransfer stage, digital image acquisition system, energy-dispersive x-ray (EDX) detector, and electron energy loss spectrometer (EELS). It has been optimized to give low detection limits for elemental microanalysis and to provide quantitative images of cells and macromolecular assemblies, while minimizing damage to beam-sensitive specimens through the use of cryotechniques and highly efficient electron detectors. The versatility of the STEM allows low-dose mapping of projected mass distributions of individual molecular assemblies at ~2 nm spatial resolution and of cryosectioned cells at ~10 nm; as a consequence of the low applied dose, the structural quality of low-dose images of tissue cryosections (nominal thickness 80 nm) is comparable to conventional embedded sections. Subsequently, quantitative analysis of elemental composition can be carried out on the same specimen using either EDX and/or EELS microanalysis. For calcium, EDX sensitivity can approach 0.3 mmol/kg dry weight, while EELS is even better, achieving within a few minutes near single-atom detectability for phosphorus as well as for calcium. More recently, new techniques have been introduced, including EELS spectrum imaging which can produce quantitative core-loss calcium maps of freeze-dried tissue cryosections.

Key Words: Scanning transmission electron microscopy, mass mapping, electron energy loss spectroscopy, electron probe x-ray microanalysis, cryosections, electron beam damage, calcium, endoplasmic reticulum, mitochondria.

*Address for correspondence:
S.B. Andrews
36/2A-21, National Institutes of Health
36 Convent Drive, Bethesda, MD 20892-4062, USA
Telephone Numbers: (301) 435-2796, 496-1296
FAX Number: (301) 480-1485
E-mail: sba@helix.nih.gov

Introduction

The scanning transmission electron microscope (STEM) equipped with a field-emission gun is a well established instrument for the determination of molecular mass ("mass mapping") (Engel, 1978; Wall and Hainfeld, 1986) as well as for high-resolution microanalysis (Isaacson and Johnson, 1975; Colliex, 1985). Over the past decade, the utility of the STEM for biological studies has been enhanced by the development of several devices (a cryotransfer/cold stage, dark-field detector system, parallel-detection electron energy loss spectrometer (EELS), and high-efficiency energy-dispersive x-ray (EDX) spectrometer) which optimize sample stability and the detection of weak spectroscopic signals originating from biological structures. The performance attainable in a STEM equipped like the VG Microscopes HB501 (VG Instruments, Beverly, MA) in our laboratories was described several years ago (Leapman and Andrews, 1991, 1992), particularly with regard to low-dose dark-field imaging of freeze-dried biological specimens, to routine EDX microanalysis of such specimens, and to analysis by parallel EELS the elemental content with near-single-atom sensitivity. More recently, there have been methodological and computational advances in EELS, including the development of "spectrum-imaging" whereby parallel spectra are acquired pixel-by-pixel in a two-dimensional map (Jeanguillaume and Colliex, 1989; Balossier *et al*., 1991; Hunt and Williams, 1991). This paper briefly reviews the established biological capabilities of the STEM, and discusses in more detail some newer applications for STEM/EELS, with particular emphasis on novel ways to measure and map subcellular calcium in tissue cryosections.

Instrumentation and Methods

Electron microscope

The dedicated STEM has a number of features that are useful as an analytical instrument for biological specimens. In particular, it has a high-brightness field-emission source that provides a sub-nanometer diameter electron probe which, when coupled to an annular dark-field

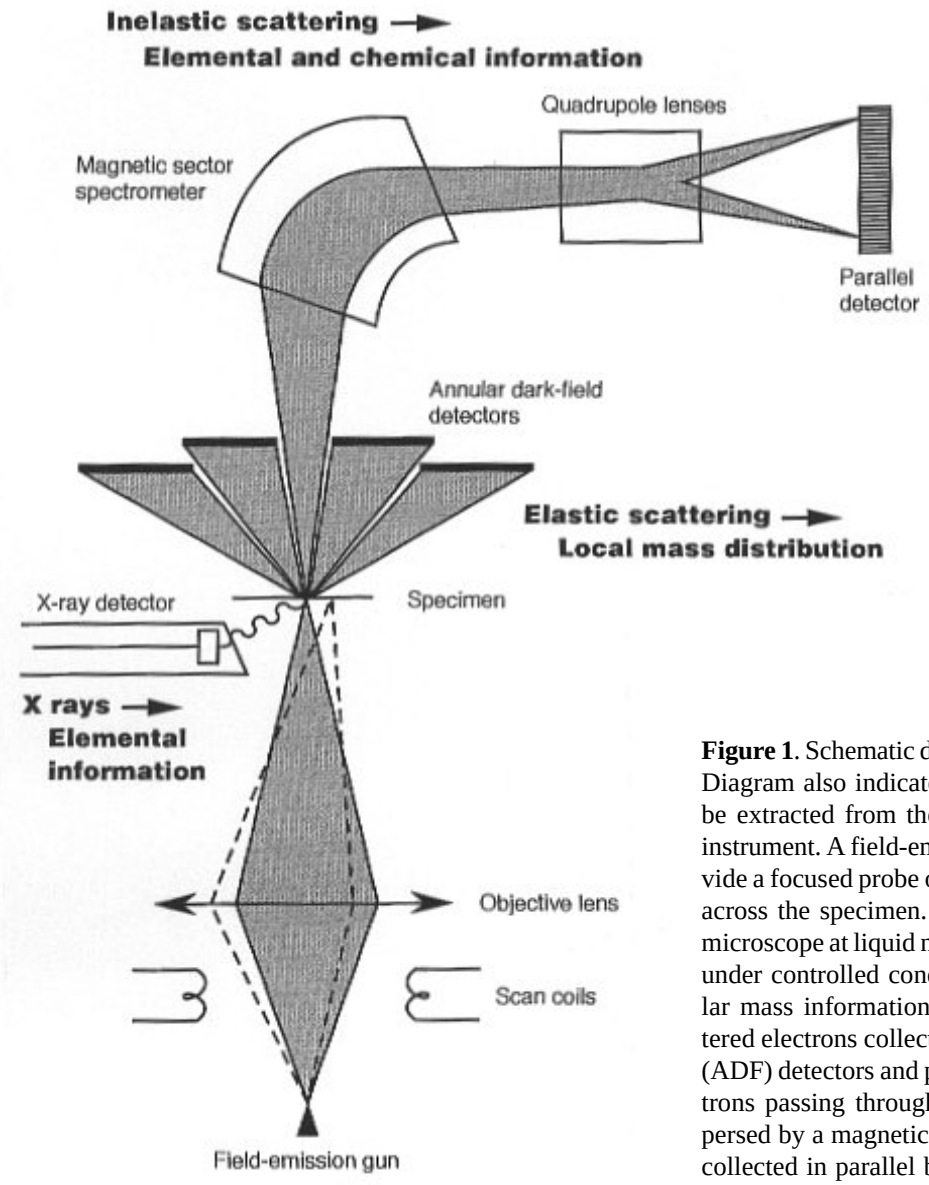

Figure 1. Schematic drawing of STEM with parallel EELS. Diagram also indicates the kinds of information that can be extracted from the different signals generated in this instrument. A field-emission source and objective lens provide a focused probe of 100 kV electrons digitally scanned across the specimen. Specimens are cryotransferred into microscope at liquid nitrogen temperature and freeze-dried under controlled conditions. Morphological and molecular mass information are obtained from elastically scattered electrons collected at low dose by annular dark-field (ADF) detectors and processed as dark-field images. Electrons passing through the ADF central aperture are dispersed by a magnetic sector spectrometer, magnified, and collected in parallel by a photodiode array coupled to an yttrium-aluminum garnet (YAG) scintillator. The EELS data so obtained are used to extract quantitative elemental information from the core-loss region as well as chemical information from the low-lose spectrum. Characteristic and continuum x-rays also generated by inelastic collisions are captured by an ultrathin window energy-dispersive detector having a collection solid angle of 0.18 steradians.

detector (ADF) that collects elastically scattered electrons with extremely high efficiency, is ideal for low-dose, dark-field imaging. The STEM also offers exciting potential as a microanalytical tool because it is capable of providing very large currents (several nanoamperes) into probe diameters of around 5 nm. Figure 1 shows a simplified schematic diagram of the system used in the present work, a VG Microscopes HB501 STEM which is operated at a beam energy of 100 keV and is equipped with a cryotransfer specimen stage, two dark-field detectors, an EDX detector, and an electron energy loss spectrometer.

Imaging

The acquisition and processing of ADF images has already been described in detail (Leapman and Andrews, 1992; Andrews *et al*., 1994). In brief, STEM images containing 1024x1024 pixels were recorded with single-electron sensitivity at a dose of ~10^3 $e^- \times nm^{-2}$ or less. Images were analyzed on Apple Macintosh desktop computers using the image processing program *IMAGE* available from W.S. Rasband at the National Institutes of Health, Bethesda, MD, USA (*http://rsb.info.nih.gov /nih-image/*).

Spectroscopy

Energy-dispersive x-ray microanalysis. Energy-dispersive x-ray spectra were acquired with a Tracor Northern (Middleton, WI) TN5500 multichannel analyzer and a Micro-ZHV ultrathin window detector having a collection solid angle of 0.18 steradian. Spectra were transferred to Macintosh computers and processed using the program *NIST/NIH DeskTop Spectrum Analyzer (DTSA)*. This software, written by C.E. Fiori, C.R. Swyt and R. Myklebust, is a dedicated program for the analysis of x-ray spectra and available for downloading at *http://micro.nist.gov/DTSA/dtsa.html*. The basis for various quantification procedures has been thoroughly reviewed (Roomans, 1988); the specific method used here is based on multiple least-squares fitting with compensation for calibration drift and peak width variability (Kitazawa *et al*., 1983).

Electron energy loss spectroscopy. EELS spectra were recorded by means of a Gatan (Warrendale, PA) model 666 electron spectrometer equipped with a 1024-channel cooled photodiode array detector coupled to a yttrium aluminum garnet (YAG) scintillator that provided a detective quantum efficiency (DQE) of ~0.3 at the high electron fluxes used here (Krivanek *et al*., 1987; Egerton *et al*., 1993). The collection semi-angle referred to the specimen was 20 mrad. In processing energy loss spectra from biological specimens it is necessary to remove the ~1% (root mean square) fixed pattern-noise caused by detector channel-to-channel gain variations. This is achieved by applying difference-acquisition techniques where spectra are shifted electrically across the detector and subtracted (Shuman and Kruit, 1985; Shuman and Somlyo, 1987). Although the read-out noise of photodiode arrays limits DQE at low dose, for analytical applications at high dose these detectors can be operated near saturation so that statistics are limited mainly by shot-noise (Krivanek *et al*., 1987; Egerton *et al*., 1993). To measure successfully weak core-edge signals, it is necessary to model the EELS background intensity as accurately as possible, allowing for plural scattering effects in thicker samples; recently devised methods to achieve this have been described (Leapman and Andrews, 1995). Finally, the spectra were quantified by fitting appropriate reference spectra. It is often useful to determine elemental ratios relative to carbon, which can then be converted into units of mmol/kg dry weight (Leapman *et al*., 1993).

EELS spectrum-images were acquired by means of a scanning system (Gatan DigiPEELS) that was interfaced to the VG Microscopes STEM in combination with special software running on a Power Macintosh computer (*Gatan Spectrum-Imaging Package*; Hunt, J.A. and Harmon, R., to be published). In this configuration, a spectrum is read out from a 1024-channel photodiode array at each pixel in a digitally rastered image. At the end of each scan line, spectral acquisition is briefly halted to acquire a rapid dark-field image. This image is cross-correlated with the previous image to correct for specimen drift; drift correction required approximately 2 sec per scan line. Typical acquisition times were 0.2 sec per pixel for a 64x64 pixel map giving a total time of about 800 seconds. The Gatan software permits quantification of the resulting spectrum-images by extrapolation of the background under core-edge peaks according to the inverse power law.

Specimen Preparation

Tissue specimens were rapidly frozen by propelling an undamaged surface of excised or cultured tissue against a liquid nitrogen-cooled sapphire block in a modified LifeCell CF100 freezing device (RMC Inc., Tucson, AZ). Specimens were frozen on specially designed, aluminum disks which were made to fit the specimen holder of a Leica Ultracut S/FCS cryoultramicrotome (Leica, Deerfield, IL) that was used to prepare cryosections. Sections were cut with a dry, 35° diamond knife (Diatome USA, Fort Washington, PA) and mounted on carbon-coated Formvar support films, essentially as described (Michel *et al*., 1992; Buchanan *et al*., 1993). For proper sectioning, an antistatic device (Hauf Static Line, Diatome USA) was essential. The nominal thickness of hydrated sections was 80 nm, although sections were actually 1.5-2.0 times thicker, mainly due to compression (Shi *et al*., 1996). After freeze-drying and mass loss, the mass thickness of the support films was ~20% that of the sections. Specimens of isolated molecules were prepared by adsorbtion from appropriate buffer onto ~3 nm carbon foils supported on copper grids. Solutions were then blotted to a thin aqueous film and plunge-frozen (Leica KF-80) in liquid ethane at -160°C. For both cryosections and frozen-hydrated molecules, grids were cryotransferred into the STEM, freeze-dried at -110°C, and recooled to -160°C for imaging and analysis.

Dark-field Imaging and Analysis

Historically, the main biological applications of STEM have involved low-dose dark-field imaging whereby molecular weights of large protein assemblies can be accurately determined. This application has been extensively reviewed, with respect to both the "mass mapping" technique in general (Engel, 1978; Wall and Hainfeld, 1986), with respect to mass and water measurement in tissue sections (Zierold, 1986; Andrews *et al*., 1994), and as practiced on our microscope (Andrews *et al*., 1994). Apart from its use as an analytical technique, low-dose dark-field imaging is extremely useful in a structural sense, especially for imaging cryosections. It is our experience that freeze-dried cryosections of tissues are rather structurally unstable, so that image quality and interpretability at the

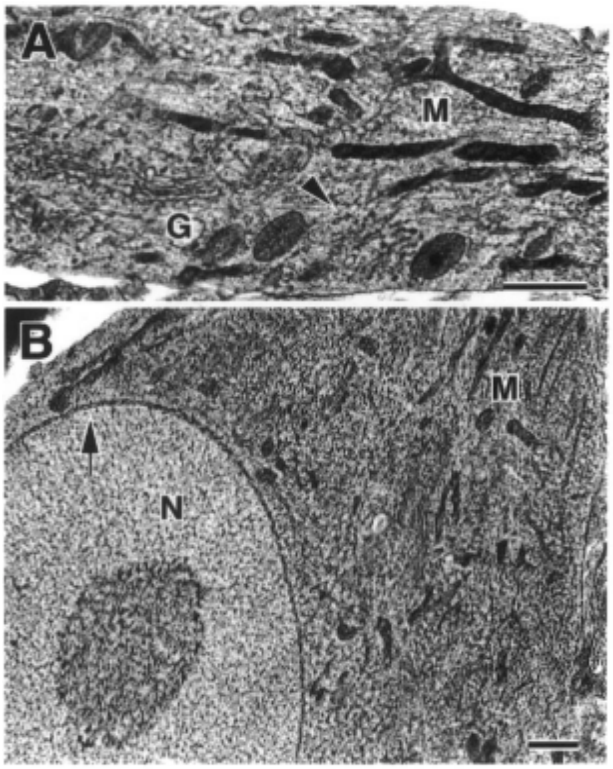

Figure 2. Low-dose, digital dark-field STEM micrographs of dendritic process (**A**) and perinuclear region of cell body (**B**) of hippocampal pyramidal neurons. The preparations were cryosections from unfixed, rapidly frozen slice cultures of rat hippocampus (Pozzo-Miller *et al*., 1997). Micrographs illustrate the morphological resolution available from good-quality cryosections. At lower magnification (panel B) large field of smoothly sectioned cell reveals larger characteristic cell features, such as nucleus (N), clusters of mitochondria (M); the bilaminar nature of the nuclear membrane is evident (arrow). With increased magnification (panel A), smaller features can be appreciated; these include cisterns of smooth endoplasmic reticulum (arrowhead) dispersed among numerous elongated mitochondria (M) and an unusually large and well-organized dendritic Golgi apparatus (G). Bars = 1 µm.

subcellular level are greatly improved by employing standard low-temperature, low-dose techniques in order to limit beam exposure. In this case, the quality and information content of cryosections of rapidly frozen tissues can be nearly as good as conventional preparations, while still retaining physiological element content and distributions (Fig. 2).

Electron Probe X-ray Microanalysis

The ability to image and identify structures in high-quality cryosections makes it feasible to carry out x-ray microanalysis at high, i.e., subcellular, resolution. In such cases, it is frequently necessary to measure very low elemental concentrations. As an example, calcium (an element of central importance in our studies) typically occurs in tissue compartments at concentrations of 1-10 mmol/kg dry weight of tissue (corresponding to 10-100 atomic parts per million) and it is ultimately desirable to measure the concentration of this element with a standard error of ± 0.1 mmol/kg (equivalent to ±1 atomic ppm). Detection of calcium in biological specimens is further complicated by the presence of relatively high levels of potassium (about 500 mmol/kg dry weight), which gives rise to overlap of the potassium K_b and calcium K_a peaks in the EDX spectrum. Although counting statistics can often be the limiting factor for detectability, this is not necessarily the case because in the analytical electron microscope it is possible to collect spectra for long periods using a high probe current. In fact, a precision of ±0.1 mmol/kg dry weight for the detection of calcium was first achieved in 1985 by Somlyo *et al*. (1985). Such experiments have demonstrated EDX detection limits that are arguably lower for biological analysis than for any other type of application. Nonetheless, there are some practical problems for obtaining this high sensitivity.

Our main point concerns the behavior of EDX pulse processing electronics. In particular, these electronics can subtly affect the x-ray peak shape as a function of count rate, thereby introducing systematic errors in the fitting procedure. Thus, although the non-linear (Simplex) method for peak fitting is optimal for many applications, it cannot account satisfactorily for non-Gaussian distortions of the K K_a and K_b peaks. For quantifying low levels of calcium it is therefore preferable to use multiple least squares (MLS) fitting of standard reference spectra. However, care must be taken to record reference spectra at the same count rate as for the unknown sample to ensure a similar peak shape. Ideally, it would be preferable to operate with low dead-time (<15%) to ensure gaussian peak shapes, but this is not always practical because the acquisition time become prohibitively long. To optimize the analysis of calcium with our Noran Micro-ZHV detector, dead-times of around 30% are required to achieve the necessary count rates.

As shown by Kitazawa *et al*. (1983), very small shifts (~1 eV) in energy calibration and resolution can affect the quality of MLS fits for the K and Ca peaks; these changes can be taken into account by incorporating first and second derivatives of the K reference spectrum. Most analysis programs operate with digitally filtered spectra to re-

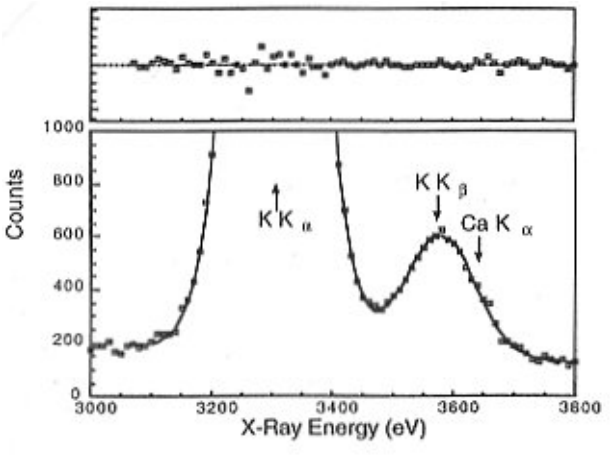

Figure 3. EDX spectrum from cryosectioned cell nucleus containing submillimolar concentration of calcium. Lower panel - Potassium/calcium region of summed spectra (20,000 sec total acquisition time) is shown to illustrate multiple least squares fit to unfiltered reference spectra. Upper panel - Residuals of the fit; reduced $\chi^2 = 0.6$. Mean Ca concentration was determined to be 0.31±0.15 mmol/kg dry weight (±SEM).

move the background, but recently we have found that an improved fit can often be achieved using unfiltered spectra along with spectra from pure carbon as a reference for the continuum. The MLS fitting procedure provides a theoretical value for the precision (± standard deviation, s.d.) as well as a measure of the quality of fit from the computed value of χ^2. However, the only reliable method for testing the accuracy of analysis at the ppm level is by careful measurements on standards. For Ca this is not a trivial task because it is difficult to prepare samples completely free of Ca contamination.

An optimized result is illustrated in Figure 3 where the unfiltered EDX spectrum (acquired with a dead-time of 35%) from the nucleus of a cryosectioned neuron has been fitted with K, Ca and C-continuum reference spectra. This fit was obtained using the program DTSA (see Instrumentation and Methods) together with other software (Kundmann *et al*., 1990). The residuals in Figure 3 indicate a high quality of fit (reduced $\chi^2 = 0.6$). By analyzing 36 such spectra (total acquisition time approximately 20,000 s), the mean Ca concentration was found to be 0.31±0.15 mmol/kg dry weight (± standard error of the mean, SEM) corresponding to an atomic concentration of 3±1.5 ppm (Leapman *et al*., 1998). In contrast, a mean calcium concentration of -0.03±0.14 was erroneously found if a K reference spectrum acquired with a deadtime of 30% instead of 35% was used. This illustrates how very minor changes in peak shape can limit accuracy at the these trace levels, even though the precision is not necessarily affected. The problem of variable peak shape is not specifically limited to calcium, but applies equally well to the analysis of other elements over a range of different specimens. Lastly, we note that 1 atomic ppm of an element in a cubic volume 30 nm on a side corresponds to only 1-3 atoms. While such fine detectability is impressive, EDX analysis demands an unrealistic investment of time to achieve this. Consequently, EELS, which offers inherently better sensitivity, is a more attractive way to attain submillimolar sensitivity, as will be discussed next.

Electron Energy Loss Spectroscopy

Recent advances in EELS have significantly extended the range of applications for biological microanalysis (Shuman and Kruit, 1985; Krivanek *et al*., 1987; Balossier *et al*., 1991; Hunt and Williams, 1991; Tang *et al*., 1994). As only one example, EELS can detect physiological concentrations of calcium in sections of rapidly frozen cells with a sensitivity 3-4x greater than that achievable by EDX (Leapman *et al*., 1993). This high intrinsic sensitivity of EELS, when coupled with recent instrumental developments, makes it possible to consider using EELS microanalysis for the detection of single atoms or ions bound to biological assemblies and organelles. Although the meaningful spatial resolution in such analyses will be limited to ~10 nm or worse by radiation damage, this rather ambitious goal, originally proposed some twenty years ago (Isaacson and Johnson, 1975), appears to be within reach. The following section gives some examples where EELS has been able to detect surprisingly small numbers of atoms in biological specimens; it further indicates some fundamental and/or practical limitations that are encountered.

Tightly and covalently bound elements

The energy-loss spectrum shown in Figure 4a was recorded from a single molecule of rapidly frozen and freeze-dried hemoglobin in 150 sec with a 4-nA probe current into an area of 80 nm^2; this corresponds to a massive incident dose of approximately $5x10^{10}$ $e^-\times nm^{-2}$. Despite drastic mass loss from the protein and even the ~3 nm thick carbon support film, as observed in dark-field STEM, the four iron atoms in a single 65 kDa hemoglobin molecule are detected by the Fe L_3 peak in the energy-loss spectrum with an uncertainty of about ±1 atom (s.d.) (Leapman and Andrews, 1992). This spectrum was recorded with a cooled photodiode array detector using the second-difference technique to correct for channel-to-channel gain variations. In our view, this EELS approach has significant potential applications in the field of cell regulation, especially the numerous and important processes that involve kinase-dependent phosphorylation. One per-

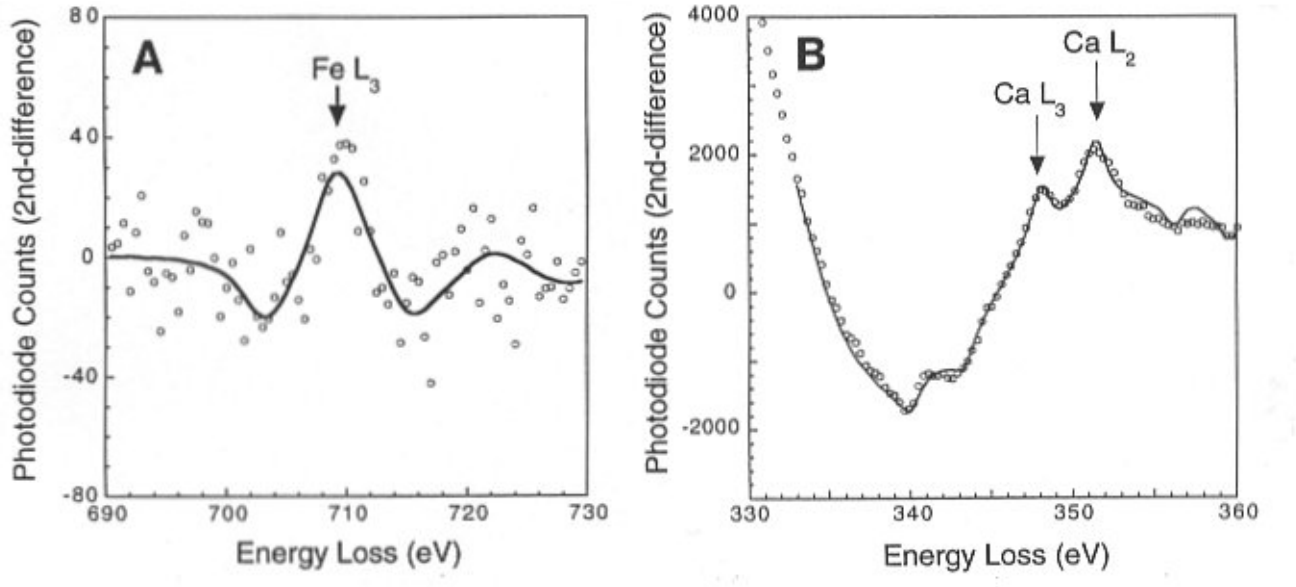

Figure 4. Detection of small numbers of atoms in biological specimens. (**A**) EELS from a single molecule of hemoglobin showing detection of four iron atoms; solid curve is fit to reference spectra. In this type of specimen, minimum detectable mass is presently limited by radiation damage. (**B**) EELS from a 30-nm diameter cistern of endoplasmic reticulum in a dendrite of cryosectioned rat hippocampal neuron, showing detection of ~20 calcium atoms at a concentration of 11±1 mmol/kg dry weight; solid curve is fit to reference spectra. For calcium, minimum detectable mass fraction is limited by inaccuracies in modeling the background.

tinent illustration is our recent measurements of the phosphorylation level of individual squid neurofilament proteins at a sensitivity of about ±5 P atoms (Leapman *et al*., 1997). Presently, this level of detection is good but not optimized. One can expect detection limits to be further improved by at least a factor of two by using two-dimensional CCD array-detectors and eliminating channel-to-channel noise by gain-normalization (Tang *et al*., 1994; Krivanek *et al*., 1995). The fundamental limitation here is beam-induced mass-loss, the most important contribution probably being due to knock-on damage of light elements (Isaacson, 1977).

Diffusible elements in tissues

Another important capability of EELS is detection of small numbers of atoms contained within larger cellular structures at trace levels of around 10-100 ppm (Shuman and Somlyo, 1987; Leapman *et al*., 1993; Leapman and Newbury, 1993). Of particular biological importance is the analysis of calcium, which has a favorably high L_{23}-ionization cross section. One example is illustrated by Figure 4b, an EELS spectrum from a single cistern of endoplasmic reticulum in a cryosectioned dendrite of rapidly frozen rat hippocampal neurons. The spectrum was recorded in 60 sec with a probe current of 3 nA into an area of 400 nm^2, again using the second-difference technique. By fitting a Ca reference spectrum it was found that the atomic ratio of Ca/C in the analytical volume was $2.5x10^{-4}$, corresponding to an estimated Ca concentration of 11±1 mmol/kg dry weight. Such sensitivity is quite good (there were only ~20 Ca atoms in the analytical volume) but the realistically achievable detection limit is much better than this. At present, the minimum detectable concentration is limited by errors in modeling the background in the vicinity of the Ca L_{23}-edge rather than by the signal-to-noise. Although plural scattering effects can be taken into account accurately, it is less straightforward to model slight variations in carbon K-edge fine structure that are weakly dependent on the matrix composition. By carefully selecting appropriate reference spectra it should be possible to measure Ca at <1 mmol/kg dry weight, corresponding to atomic concentrations in the ppm range with acquisition times on the order of a few minutes. This represents a major savings in time and dose relative to EDX analysis.

Quantitative element mapping

It is evidently desirable to quantitatively map, rather than just point analyze, the distribution of physiologically important element at subcellular resolution. Mapping provides an intuitively useful structural context for numerical, analytical data, and further obviates the need for subjectively choosing a few locations for analysis in the hope

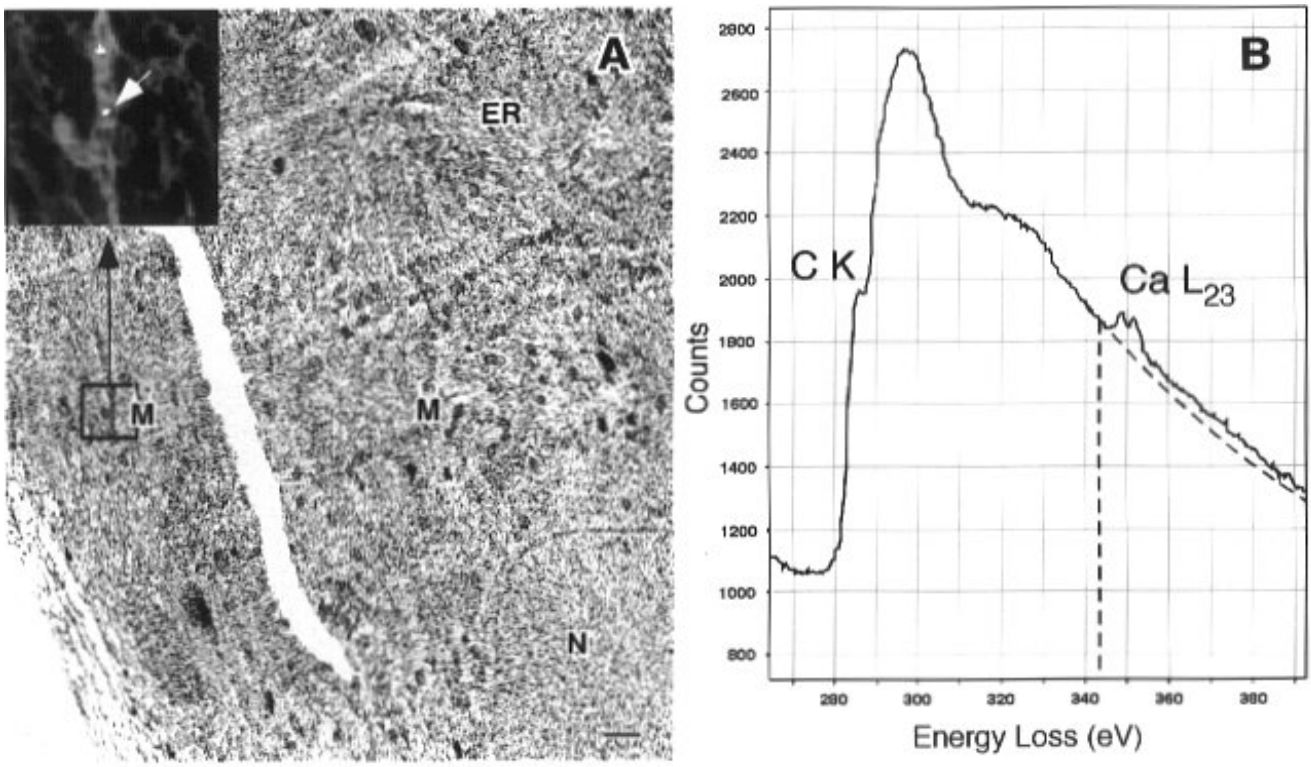

Figure 5. Spectrum-imaging of calcium accumulation in certain mitochondria of depolarized sympathetic neurons. (**A**) Low-dose, dark-field STEM micrograph of soma of rapidly frozen neuron from isolated frog sympathetic ganglion. This low-power micrograph shows the abundant mitochondria (M) dispersed throughout perinuclear (N, nucleus) cytoplasm; clusters of endoplasmic reticulum (ER) are also present, but difficult to appreciate at this resolution. Square at left marks region near cell plasma membrane containing two abutted mitochondria from which spectrum-image was obtained. White diagonal slash is a crack in the cryosection. Bar = 1 μm. (**B**) EELS from one 20-nm diameter pixel (actual pixel indicated by arrow on inset of panel A) within a peripheral mitochondrion. Spectrum shows a very prominent Ca L_{23} edge; fit of background intensity according to power-law extrapolation of pre-edge intensities is indicated by dotted line. (**A, inset**) 64x64-pixel calcium map (white) overlaid on a nitrogen map from indicated region containing two mitochondria. Visual maps were generated by fitting each pixel individually, and subsequently scaling minimum/maximum values (0-~3000 counts) to 256 gray levels. Quantitative values were derived from Ca/C ratios, as previously described (Leapman *et al*., 1993).

that these are representative of the cell as a whole. There are two complementary approaches to element mapping: STEM/EELS spectrum-imaging (Jeanguillaume and Colliex, 1989) and energy-filtered transmission EM (EFTEM) (Ottensmeyer, 1984; Krivanek *et al*., 1995). When local elemental concentrations are relatively high, e.g., phosphorus in DNA (Bazett-Jones *et al*., 1994), the EFTEM can offer some advantages over the STEM. In EFTEM entire inelastic images are recorded in parallel by means of a two-dimensional detector [e.g., a coupled charge device (CCD) array] but the spectral information must be recorded serially one energy loss at a time. Efficient, cooled slow-scan CCD cameras used in conjunction with a variety of EFTEM systems provide quantitative images with low detector noise (Krivanek *et al*., 1995; Probst and Bayer, 1995). It is possible to record sequences of energy-selected images containing 1024x1024-pixels in acquisition times of only a few minutes or less, from which elemental maps can be computed by extrapolating and then subtracting the background under the core edges. An equivalent STEM spectrum-image, that is, a collection of complete energy loss spectra at each pixel in a scanned image (Jeanguillaume and Colliex, 1989), would require several hours to acquire with a typical minimum integration time of 25 ms per pixel. Nonetheless, STEM spectrum-imaging is essential for applications involving detection of physi-

ologically relevant concentrations of calcium in rapidly-frozen, cryosectioned tissue. This is because very precise background modeling must be used to extract the very weak Ca signal.

In cases where spatially averaged Ca concentrations are either satisfactory or desirable, the spatial plane (x-y plane) of the spectrum-image data set can be segmented into regions of interest, and selected spectra summed to give $>10^7$ scattered electrons per channel in an integrated spectrum. This approach provides, at high sensitivity and resolution, spatially averaged information about total calcium concentrations. Although not truly a map, such information is nonetheless physiologically useful for comparison with other spatial averaging techniques such as measurements of free Ca^{2+} with fluorescent probes. We have used the summed spectrum-image approach to measure Ca with a sensitivity <1 mmol/kg dry weight in cerebellar neurons (Leapman *et al*., 1993).

Evidently, when the local concentration is high enough, spectrum-imaging can potentially reveal the quantitative distribution of calcium at single pixel resolution. Until recently, this has been of minimal value in physiology, mainly because, with few exceptions (Somlyo, 1984), intracellular calcium does not occur in concentrations high enough to reach detection thresholds in a 100-ms EELS acquisition. However, it has recently been discovered that intraorganelle total Ca transiently reaches remarkably high levels, sometimes exceeding 100 mmol/kg dry weight, during depolarization-induced Ca^{2+} entry in certain neurons (Pozzo-Miller *et al*., 1997). While the endoplasmic reticulum is clearly the dominant Ca-accumulating organelle in hippocampal neurons, we have recently found that sympathetic neurons prefer to accumulate Ca within their abundant mitochondria (unpublished results). In these cells, some local concentrations of intramitochondrial Ca reached after a 2 min depolarization are sufficiently high to allow direct mapping, pixel by pixel, by means of EELS spectrum-imaging. The 64x64 pixel, 256 gray-level true Ca map in Figure 5a (inset) reveals the accumulation of Ca in 20 nm, phosphorus-rich inclusions within one of two mitochondria in a depolarized sympathetic neuron. The Ca concentration within the inclusions was so high that the prominent Ca L_{23}-edge in a single-pixel spectrum could be satisfactorily processed by simple extrapolation of the pre-edge background, as shown (Fig. 5b). Quantitation indicates that the Ca concentration was ~600 mmol/kg dry weight, while the concentration integrated over the whole mitochondrion was ~30 mmol/kg; the latter value is in good agreement with parallel measurements by EDX microanalysis. In the case of single-pixel spectra with Ca edges corresponding to concentrations of around 50 mmol/kg, the edge could still be readily fit using the MLS techniques mentioned above. The future challenge is to develop acquisition and processing techniques that will allow quantitation of single-pixel spectra representing Ca concentrations <10 mmol/kg dry weight, which is the concentration range for the vast majority of cellular compartments.

Summary

The unique demands of analyzing biological specimens have proven very helpful for advancing STEM instrumentation and techniques. A modern STEM in a biological setting can now combine cryotechniques, low-dose quantitative imaging and complementary types of microanalysis to achieve a detailed, high-resolution characterization of a protein, cell, or cell assembly, all in one integrated instrument. Perhaps the most promising area of progress has been EELS, where recent advances have significantly extended the scope of biological applications. Thus, STEM/EELS has demonstrated a sensitivity of only a few atoms for several relevant types of biological preparations, one specific example being the detection of ~10 phosphorus atoms in a single measurement from a 10 nm segment of a neurofilament (Leapman *et al*., 1997). Such high sensitivity is especially promising for the analysis of calcium. In the case of this important element, parallel EELS provides a sensitivity improvement of about four relative to EDX (Shuman and Somlyo, 1987; Leapman *et al*., 1993), which is particularly significant because calcium is often present at levels that are only just detectable by EDX. Another promising advance is the maturation of spectrum-imaging, a technique which allows maximum flexibility in data processing and evaluation, and opens up the prospect of true quantitative elemental mapping. Although this paper has focused on elemental analysis, it should be noted that detailed chemical information is also obtainable from the valence excitation EEL spectrum which, to give one example, has been used to map the water content in subcellular compartments of frozen-hydrated cryosections (Sun *et al*., 1993).

With regard to future prospects, one anticipated improvement would be the development of parallel detectors with higher detective quantum efficiency and faster readout so that data can be acquired more rapidly from beam-sensitive specimens. An improvement of at least a factor of two can be expected from more efficient CCD detectors (Tang *et al*., 1994). In the final analysis, however, the ultimate limits will still be dictated by radiation damage to the specimen. In principle, it should be possible to detect single atoms of calcium or phosphorus in 10-nm diameter analytical volumes, but the required dose for such single-atom detection is about one order of magnitude greater than that necessary for complete loss of the organic matrix. Such considerations place a premium on continuing efforts to extract the maximum amount signal from specimen/beam interactions.

Acknowledgments

The authors are grateful to Drs. John Hunt, Carol Swyt, Tom Reese, Ghislain Nicaise and Stanley Sun for helpful discussions and advice, and to Drs. David Friel and Denes Agoston for sharing prepublication data. We also thank Shanling Shi and Maureen O'Connell for excellent technical assistance.

References

Andrews SB, Buchanan RA, Leapman RD (1994) Quantitative dark-field mass analysis of ultrathin cryosections in the field-emission STEM. Scanning Microsc (Suppl) **8**:13-24.

Balossier G, Thomas X, Michel J, Wagner D, Bonnehomme P, Puchelle E, Ploton D, Bonnehomme A, Pinon JM (1991) Parallel EELS elemental mapping in scanning transmission electron microscopy: Use of the difference method. Microsc Microanal Microstruct **2**:531-546.

Bazett-Jones DP, Leblanc B, Herfort M, Moss T (1994) Short-range DNA looping by the Xenopus HMG-box transcription factor, xUBF. Science **264**:1134-1137.

Buchanan RA, Leapman RD, O'Connell MF, Reese TS, Andrews SB (1993) Quantitative scanning transmission electron microscopy of ultrathin cryosections: subcellular organelles in rapidly frozen liver and cerebellar cortex. J Struct Biol **110**: 244-255.

Colliex C (1985) An illustrated review of various factors governing the high spatial resolution capabilities in EELS microanalysis. Ultramicroscopy **18**: 131-150.

Egerton RF, Yang YY, Cheng SC (1993) Characterization and use of the Gatan 666 parallel-recording electron energy-loss spectrometer. Ultramicroscopy **48**: 239-250.

Engel A (1978) Molecular weight determination by scanning transmission electron microscopy. Ultramicroscopy **3**: 273-281.

Hunt J, Williams DB (1991) Electron energy-loss spectrum-imaging. Ultramicroscopy **38**: 47-73.

Isaacson MS (1977) Specimen damage in the electron microscope. In: Principles and Techniques of Electron Microscopy (Hayat MA, ed). Van Nostrand Reinhold, New York. pp. 1-78.

Isaacson MS, Johnson D (1975) Low Z elemental analysis using energy loss electrons. Ultramicroscopy **1**: 33-52.

Jeanguillaume C, Colliex C (1989) Spectrum-image: the next step in EELS digital acquisition and processing. Ultramicroscopy **28**: 252-257.

Kitazawa T, Shuman H, Somlyo AP (1983) Quantitative electron probe analysis: Problems and solutions. Ultramicroscopy **11**: 251-250.

Krivanek OL, Ahn CC, Keeney RB (1987) Parallel detection electron spectrometer using quadropole lenses. Ultramicroscopy **22**: 103-116.

Krivanek OL, Friedman SL, Gubbens AJ, Kraus B (1995) An imaging filter for biological applications. Ultramicroscopy **59**: 267-282.

Kundmann M, Chabert X, Truong K, Krivanek O (1990) EL/P software for Macintosh II computer, Gatan, Inc., Pleasanton, CA, USA.

Leapman RD, Andrews SB (1991) Analysis of directly frozen macromolecules and tissues in the field-emission STEM. J Microsc **161**: 3-19.

Leapman RD, Andrews SB (1992) Characterization of biological macromolecules by combined mass mapping and electron energy-loss spectroscopy. J Microsc **165**: 225-238.

Leapman RD, Andrews SB (1995) Improved method for quantifying EELS difference spectra from biological specimens. In: Proc 29th Ann MAS Mtg (Etz ES, ed). VCH Publishers, New York. pp. 331-332.

Leapman RD, Gallant PE, Reese TS, Andrews SB (1997) Phosphorylation and subunit organization of axonal neurofilaments determined by scanning transmission electron microscopy. Proc Natl Acad Sci U S A **94**: 7820-7824.

Leapman RD, Hunt JA, Buchanan RA, Andrews SB (1993) Measurement of low calcium concentrations in cryosectioned cells by parallel-EELS mapping. Ultramicroscopy **49**: 225-234.

Leapman RD, Newbury DE (1993) Trace elemental analysis at nanometer spatial resolution by parallel- detection electron energy loss spectroscopy. Anal Chem **65**: 2409-2414.

Leapman RD, Swyt-Thomas CR, Agoston DV, Pivovarova NB, Andrews SB (1998) Trace element quantitation in biological x-ray microanalysis. Microscopy and Microanalysis. Bailey GW, Alexander RB, Jerome WG, Bond MG, McCarthy JJ (eds). Springer-Verlag, New York. pp. 212-213.

Michel M, Gnägi H, Müller M (1992) Diamonds are a cryosectioner's best friend. J Microsc **166**: 43-56.

Ottensmeyer FP (1984) Electron spectroscopic imaging: parallel energy filtering and microanalysis in the fixed-beam electron microscope. J Ultrastruct Res **88**: 121-134.

Pozzo-Miller LD, Pivovarova NB, Leapman RD, Buchanan RA, Reese TS, Andrews SB (1997) Activity-dependent calcium sequestration in dendrites of hippocampal neurons in brain slices. J Neurosci **17**: 8729-8738.

Probst W, Bayer VE (1995) The energy filtering TEM (EFTEM) in modern biological transmission electron microscopy. Proc Microscopy and Microanalysis 1995 (Bailey GW, Ellisman MH, Hennigar RA, Zaluzec NJ, eds).

Jones and Begell, New York. pp. 668-669.

Roomans GM (1988) Quantitative x-ray microanalysis of biological specimens. J Electron Microsc Techn **9**: 19-43.

Shi S, Sun S, Andrews SB, Leapman RD (1996) Thickness measurement of hydrated and dehydrated cryosections by EELS. Microsc Res Techn **33**: 241-250.

Shuman H, Kruit P (1985) Quantitative data processing of parallel recorded electron energy loss spectra with low signal to background. Rev Sci Instrum **56**: 231-239.

Shuman H, Somlyo AP (1987) Electron energy loss analysis of near-trace-element concentrations of calcium. Ultramicroscopy **21**: 23-32.

Somlyo AP (1984) Compositional mapping in biology: X rays and electrons. J Ultrastruct Res **88**: 135-142.

Somlyo AP, Bond M, Somlyo AV (1985) Calcium content of mitochondria and endoplasmic reticulum in liver rapidly frozen in vivo. Nature **314**: 622-625.

Sun S, Shi SL, Leapman RD (1993) Water distributions of hydrated biological specimens by valence electron energy loss spectroscopy. Ultramicroscopy **50**: 127-139.

Tang Z, Ho R, Xu Z, Shao Z, Somlyo AP (1994) A high-sensitivity CCD system for parallel electron energy-loss spectroscopy (CCD for EELS). J Microsc **175**: 100-107.

Wall JS, Hainfeld JF (1986) Mass mapping with the scanning transmission electron microscope. Annu Rev Biophys Biophys Chem **15**: 355-376.

Zierold K (1986) The determination of wet weight concentrations of elements in freeze-dried cryosections from biological cells. Scanning Electron Microsc 1986; II: 713-724.

Discussion with Reviewers

G.M. Roomans: The presence of particles containing high Ca and high P in mitochondria has generally been associated with pathological conditions. Do the authors assume or have evidence that this calcium accumulation is reversible or does calcium accumulation irreversibly damage the mitochondria?

Authors: The reviewer is correct in noting the considerable literature that associates Ca- and P-rich precipitates with cell damage and even death. However, the punctate accumulation of Ca described in our experiments appears to be more physiological than pathological for at least two reasons: (1) Formation of Ca-rich inclusions within mitochondria of sympathetic neurons was evoked using a depolarization protocol (50 mM K^+ for 2 min) that is known to reversibly increase cytoplasmic free Ca^{2+} only into the normal physiological range of 500-700 nM (Friel and Tsien (1994); (2) more directly, Ca-rich inclusions were no longer present, and mitochondrial total Ca content had returned to baseline, after a 5 min recovery period. Further, there were no morphological changes in mitchondria following a cycle of Ca uptake and release. These observations strongly imply that the Ca- and P-rich inclusions are readily resoluble, although their chemical nature is not well understood.

G.M. Roomans: What is the advantage of the sapphire in the cryo-slamming device over the conventional gold-plated copper?

Authors: Sapphire has the the advantage of presenting a hard and molecularly smooth freezing surface, one which is not subject to nicking (like gold) or oxidation (like copper).

R. Wróblewski: In your EDX system, beam currents giving deadtimes around 30% are used to achieve the necessary number of counts. You also state that lowering the deadtime by 5% caused significant changes in peak shapes, so that calcium could no longer be fit with the original reference spectra. Is it better to increase the beam intensity to give deadtimes around 35%, or better to use a longer time of analysis with a lower deadtime?

Authors: In our view, it is always better when analyzing for calcium to maximize the number of characteristic counts. However, it is self-defeating to increase the count rate to the point where deadtime effects cause peak shape distortions which preclude accurate fitting. In the EDX system of our VG STEM, spectra obtained with deadtimes of 35% represent a reasonable combination of count rate, resolution and reproducible peak shape.

R. Wróblewski: The EELS analysis of the mitochondrial inclusions found after neuron depolarization showed that they were Ca and P rich. Could you detect P and Ca simultaneously in your EELS spectra?

Authors: Yes, EELS from the mitochondrial inclusions showed both Ca and P L_{23}-edges consistent with some form of calcium phosphate.

K. Zierold: In cryosectioned cells often the nuclear membrane is imaged more clearly than the cell membrane, as in your Figure 2. Can you explain this effect?

Authors: Not with any certainty, but we can speculate. One possibility is that the double membrane of the nuclear envelope is delineated better than the single bilayer membrane of the plasmalemma. A related consideration is the usual presence of a significant sub-plasmalemmal cytoskeleton, which could tend to obscure the membrane *per se*. In addition, cryosections are known to shrink substantially during freeze-dried, often with consequent tearing or folding of the section. This artifact occurs preferentially at

structurally weak areas, including the interface between the cell periphery and the extracellular space. As a result, the plasma membrane is often contained within a distorted region.

K. Zierold: Your Figure 4A shows an EELS spectrum of a single hemoglobin molecule. Do you obtain similar EELS spectra from cryosectioned red blood cells?
Authors: Yes, EELS data from cryosectioned red blood cells also show a clear Fe L_{23} edge, as expected.

K. Zierold: If you compare the EELS Ca spectra in Figures 4B and 5B with corresponding EDX spectra, do you obtain similar quantitative results?
Authors: Yes, the quantitation of EELS spectrum in Figure 5b indicates the Ca concentration in the inclusion is very high, ~600 mmol/kg dry weight, but the spatially averaged concentration over the whole mitochondrion is ~30 mmol/kg dry weight. The latter value is in agreement with EDX measurements.

K. Zierold: Do you see any chance for (high resolution) analytical electron microscopy of frozen hydrated specimens, in particular of cryosections?
Authors: This would seem to be beyond the current capabilities of analytical microscopy. We have previously shown (Leapman and Andrews, 1991) that it is feasible to obtain quantitatively useful EDX spectra from hydrated specimens, but only at micrometer resolution. The high radiation sensitivity of hydrated biological specimens limits doses to $<10^4$ e^-/nm^2, which in turn limits counting statistics.

Additional Reference

Friel DD, Tsien RW (1994) An FCCP-sensitive Ca^{2+} store in bullfrog sympathetic neurons and its participation in stimulus-invoked changes in $[Ca^{2+}]_i$. J Neurosci **14**: 4007-4024.